

# Intercomparison of Terrestrial Carbon Fluxes and Carbon Use Efficiency Simulated by CMIP5 Earth System Models

Dongmin Kim<sup>1</sup>, Myong-In Lee<sup>1</sup>, Su-Jong Jeong<sup>2</sup>, Jungho Im<sup>1</sup>, Dong Hyun Cha<sup>1</sup>, and Sanggyun Lee<sup>1</sup>

<sup>1</sup>*School of Urban and Environmental Engineering, Ulsan National Institute of Science and Technology, Ulsan, Korea*

<sup>2</sup>*School of Environmental Science and Engineering, Southern University of Science and Technology, Nanshan, Shenzhen, Guangdong, China*

(Manuscript received 18 May 2017; accepted 7 July 2017)

© The Korean Meteorological Society and Springer 2017

**Abstract:** This study compares historical simulations of the terrestrial carbon cycle produced by 10 Earth System Models (ESMs) that participated in the fifth phase of the Coupled Model Intercomparison Project (CMIP5). Using MODIS satellite estimates, this study validates the simulation of gross primary production (GPP), net primary production (NPP), and carbon use efficiency (CUE), which depend on plant function types (PFTs). The models show noticeable deficiencies compared to the MODIS data in the simulation of the spatial patterns of GPP and NPP and large differences among the simulations, although the multi-model ensemble (MME) mean provides a realistic global mean value and spatial distributions. The larger model spreads in GPP and NPP compared to those of surface temperature and precipitation suggest that the differences among simulations in terms of the terrestrial carbon cycle are largely due to uncertainties in the parameterization of terrestrial carbon fluxes by vegetation. The models also exhibit large spatial differences in their simulated CUE values and at locations where the dominant PFT changes, primarily due to differences in the parameterizations. While the MME-simulated CUE values show a strong dependence on surface temperatures, the observed CUE values from MODIS show greater complexity, as well as non-linear sensitivity. This leads to the overall underestimation of CUE using most of the PFTs incorporated into current ESMs. The results of this comparison suggest that more careful and extensive validation is needed to improve the terrestrial carbon cycle in terms of ecosystem-level processes.

**Key words:** Earth system models, carbon use efficiency, CMIP5, MODIS, gross primary production, net primary production

## 1. Introduction

Earth system models (ESMs) have been developed in the past several decades to simulate vegetation changes in space and time through carbon cycle-related interactions between the biosphere and the atmosphere. The temporal variations in atmospheric CO<sub>2</sub> in the models are driven by CO<sub>2</sub> emissions from natural and anthropogenic sources, as well as uptake by vegetated land surfaces and the ocean. Net imbalances in carbon fluxes drive the secular trend in CO<sub>2</sub>. The magnitude of the imbalance is model-dependent and results in differences in

the future warming projected by various ESMs. Previous studies showed that the observed trend of atmospheric CO<sub>2</sub> was not reproduced correctly during the past century, given the historical record. There was also substantial spread among models, even though they were forced by identical anthropogenic emissions (Friedlingstein et al., 2006, 2014; Hoffman et al., 2013; Zhao and Zeng, 2014). The model bias persists into their future projections. Hoffman et al. (2013) pointed out that the spread of projected CO<sub>2</sub> concentrations among fifteen Coupled Model Intercomparison Project (CMIP5; Taylor et al., 2012) ESMs in 2100 was approximately 20% of their multi-model average. Friedlingstein et al. (2014) showed that the degree of surface temperature warming by 2100 was different by more than a factor of two, depending on the models and representative concentration pathway (RCP) 8.5 scenarios used.

Previous studies (Friedlingstein et al., 2006, 2014; Booth et al., 2012; Anav et al., 2013; Arora et al., 2013; Hoffman et al., 2013) have suggested that the uncertainty in CO<sub>2</sub> concentrations simulated by ESMs should be largely attributed to the terrestrial carbon uptake, rather than to the uptake by ocean. Hoffman et al. (2013) and Friedlingstein et al. (2014) compared the carbon uptake by land and ocean, simulated by ESMs and found that the amount of carbon accumulated by the ocean is positive in all models by 2100, whereas the models exhibited a large spread in the amount of carbon taken up by the land; the results even had different signs. Arora et al. (2013) indicated that the simulated sensitivity of terrestrial carbon storage to the atmospheric CO<sub>2</sub> concentration was 3–4 times larger than that of ocean. This suggests that the terrestrial carbon cycle is one of the important factors that need improvement for minimizing uncertainty in future climate predictions.

It is generally recognized that changes in the carbon pools in the biosphere should play a key role in determining atmospheric CO<sub>2</sub> concentration levels in the future. Shao et al. (2013) showed that the net biome production (NBP) simulated by CMIP5 ESMs is enhanced in the 21st century and that the biomass particularly increases over tropical rainforests and vegetated surfaces in the mid-latitudes through the CO<sub>2</sub> fertilization effect. Not only long-term increases in biomass but also future changes in its seasonal cycle would significantly affect CO<sub>2</sub> concentrations. Zhao and Zeng (2014) indicated that the amplitude of the seasonal cycle of atmospheric CO<sub>2</sub>

Corresponding Author: Myong-In Lee, School of Urban and Environmental Engineering, Ulsan National Institute of Science and Technology, 50 UNIST-gil, Ulsan 44919, Korea  
E-mail: milee@unist.ac.kr

tends to increase in the future, due to an increase of 68% in the seasonal cycle of NBP during the growing season in their future simulations. Comprehensive model intercomparisons on the simulation of biome production at various ecosystem levels are needed to explain the differences among simulations and minimize projection uncertainties.

The exchange of carbon between the atmosphere and terrestrial ecosystems consists of complicated biogeochemical processes operating over a heterogeneous surface, and the quality and the performance of the global model simulations is often diagnosed using carbon cycle variables such as gross primary production (GPP) and autotrophic respiration (Ra) by plants. Net primary production (NPP) is defined as GPP minus Ra. Heterotrophic respiration (Rh), involving the decomposition of soil litter, is also an important process involved in the carbon cycle. By validation using ground and satellite observational data, previous studies identified the systematic biases of ESMs and discussed the possible reasons for these biases. Anav et al. (2013) indicated that current ESMs tend to overestimate terrestrial biomass and global GPP (Anav et al., 2013). Shao et al. (2013) showed that ESMs exhibit large disagreements in the relationship between carbon cycle variables and hydrological variables, such as precipitation and soil moisture, emphasizing the importance of the hydrological cycle in terms of its effects on the terrestrial carbon cycle. The simulated soil carbon amount in the subsurface root zone, which is the major source of plant growth, showed systematic biases and large model spread, from 40 to 240%, compared with observational data (Todd-Brown et al., 2013). That study suggested that it might be responsible for the large spread of atmospheric CO<sub>2</sub> concentrations simulated by the models.

While most previous intercomparison studies involving ESMs have focused on the validation of the global mean budget of terrestrial carbon pools and fluxes (Anav et al., 2013; Shao et al., 2013; Todd-Brown et al., 2013), which is useful for evaluating the overall performance of ESMs and quantifying simulation uncertainties, more detailed analyses addressing regional scales and different vegetation types are needed to identify the key sources of systematic biases in the models. Anav et al. (2013) evaluated regional changes in biogeochemical variables for two hemispheres and the tropical region separately. In particular, an investigation of systematic biases in different types of ecosystems is required to improve the existing parameterizations of terrestrial carbon fluxes by vegetation. In contrast to the many observational studies in biology that address various plant function type (PFT) levels (De Lucia et al., 2007; Zhang et al., 2009; Zhang et al., 2014), studies that benchmark model simulations of PFT levels have obtained less attention, and this is one of the primary motivations of this study.

For a better elucidation of systematic biases in the models, this study focuses particularly on the comparison of carbon use efficiency (CUE), which is sensitive to the various PFTs. For the short-term carbon cycle, Ra is a primary measure of the release of carbon to the atmosphere, and its magnitude is

known to be about half of GPP for most vegetated surfaces (King, 2006; Piao et al., 2010). CUE is defined as the ratio of NPP to GPP, which is a useful diagnostic measure for the comparison of parameterizations for the terrestrial carbon fluxes driven by vegetation that are implemented differently in current ESMs. The absolute magnitudes of the production terms are the results of feedbacks between climate and vegetation. Normalized flux terms can highlight the differences among simulations driven by parameterization differences in terrestrial carbon fluxes. Previous studies based on in situ (De Lucia et al., 2007) and satellite (Zhang et al., 2009) data analyses have indicated that CUE is not a constant with a value of approximately 0.47 (Gifford, 1994; Dewar et al., 1999) but varies depending on climatic conditions and PFTs. In this regard, the Moderate Resolution Imaging Spectroradiometer (MODIS) satellite data provide the global coverage of GPP and NPP as a useful reference for the model validation for CUE at the PFT level. Zhang et al. (2014) suggested observed CUE by MODIS tends to slightly increase in the recent years. However, MODIS has been debated for using validation for ESMs due to uncertainty of the biomass types and meteorological data to derive GPP and NPP. To warrant for using MODIS dataset, we compared MODIS GPP and GPP from in-situ station data using previous studies and this study (section 2a).

The purpose of this study is the intercomparison of CMIP5 ESMs in terms of their simulations of the terrestrial carbon cycle, based on a quantitative evaluation of the performance of terrestrial carbon flux parameterizations in their land surface models (LSM). This analysis specifically focuses on the assessment of CUE at the PFT level and makes an effort to provide useful suggestions to the modeling community for reducing systematic biases in the terrestrial carbon cycle in current ESMs. Although the heterotrophic respiration (Rh) needs to be examined to close the terrestrial carbon budget (Bond-Lamberty and Thomson, 2010), this study does not include the analysis due to a lack of reliable reference data from observations. This study consists of following sections: Section 2 describes the observational data and model output used in this study. Section 3 compares the model simulations in terms of their climate and terrestrial carbon cycle variables, comparing first the multi-model ensemble (MME) average to diagnose common and systematic biases in the current models and then identifies differences among simulations across the ESMs in their simulated climates and carbon fluxes. The comparison of CUE at various PFT levels is followed by more comprehensive comparisons for identifying differences among simulations driven by model parameterizations. Finally, Section 4 provides a summary and conclusions.

## 2. Data and analysis methods

### a. Observational data

This study used GPP and NPP as primary variables to validate the global carbon cycle as simulated by various

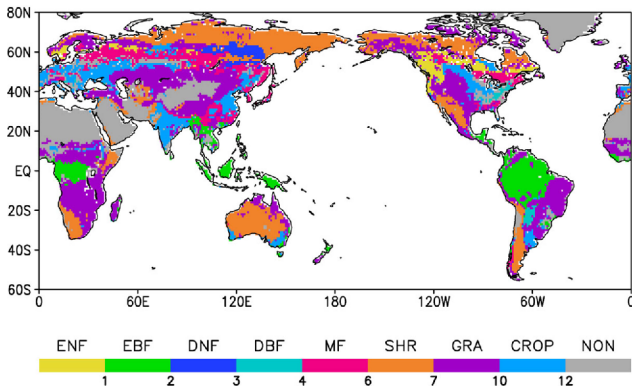


**Fig. 1.** Horizontal distribution of dominant plant function types (PFTs) using the MODIS land cover data that include evergreen needleleaf forest (ENF), evergreen broadleaf forest (EBF), deciduous needleleaf forest (DNF), deciduous broadleaf (DBF), mixed forest (MF), shrub land (SHR), grass (GRA), cropland (CROP) and non-vegetated area (NON).

ESMs. Reference observational data were obtained from the NASA MODIS MOD17 data product, which includes the first satellite-driven estimates of carbon fluxes on vegetated surfaces on a global scale (Running and Gower, 1991; Zhao et al., 2005).

The MODIS algorithm uses a data model based on the radiation use efficiency logic of Monteith (1972) to estimate GPP, which is basically a linear function of the amount of Photosynthetically Active Radiation (PAR) absorbed. The fraction of PAR and the leaf area index (LAI) are provided to the model by the MODIS MOD15 products. A conversion efficiency parameter relating absorbed radiation to the actual productivity depends on vegetation type and climate condition. The upper limit of conversion efficiency uses the Biome Parameter Lookup Table (BPLUT) for different vegetation types. The vegetation types include evergreen needleleaf forest (ENF), evergreen broadleaf forest (EBF), deciduous needleleaf forest (DNF), deciduous broadleaf forest (DBF), mixed forests (MF), open and closed shrublands (SHR), grasslands (GRA), and croplands (CROP), which are based on the land cover classification from the MODIS MCD12Q1 ([https://lpdaac.usgs.gov/dataset\\_discovery/modis/modis\\_products\\_table/mcd12q1](https://lpdaac.usgs.gov/dataset_discovery/modis/modis_products_table/mcd12q1)). Figure 1 shows the horizontal distribution of vegetation types from MODIS. The conversion efficiency is modified by climate conditions such as incoming solar radiation, temperature, and vapor pressure deficit, which are obtained from atmospheric reanalyses developed by NASA's Global Modeling and Assimilation Office and the NCEP/NCAR Reanalysis II. The NPP estimation by MODIS calculates daily leaf and fine root maintenance respiration, annual growth respiration, and annual maintenance respiration of live cells in woody tissue, which are subtracted from the GPP. Biome-specific physiological parameters are also specified by BPLUT for respiration calculations.

The MOD17 dataset provides 8-day, monthly, and annual mean GPP and NPP for 2000–2012. This study used the

gridded GPP and NPP products, which have a spatial resolution of 30 arcsec (0.0083 degree), provided by the Numerical Terradynamic Simulation Group (NTSG) of the University of Montana (NTSG MOD17 v55).

Although MODIS is affected by uncertainties in biomass types and meteorological data sets (Zhao et al., 2005), the derived GPP and NPP values are able to capture realistic spatial and temporal variations over different biomes and climate regimes. Heinsch et al. (2006) demonstrated that the data are consistent with ground-based flux tower measurements of GPP and field-observed NPP estimates with high correlation ( $r = 0.86$ ) between the data containing seasonal variation. When this study also compared the annual gridded MODIS GPP data averaged for 6 years (2000–2005) with the nearest station data from 53 FLUXNET tower sites, the  $r$ -squared value was as high as 0.56. This value is comparable with the ones in other studies (Zhao et al., 2005; Turner et al., 2006), showing the gridded MODIS data are reliable for the model evaluation.

For comparison with MODIS, this study also used GPP estimates from FLUXNET-MTE (Multi-Tree Ensemble; Jung et al., 2011), which is an upscaled data set providing global coverage that is derived from 178 surface flux tower observations using a machine learning technique. FLUXNET-MTE provides an explicit estimate of carbon fluxes over vegetated surfaces. The dataset provides monthly data at a  $0.5^\circ \times 0.5^\circ$  (latitude  $\times$  longitude) spatial resolution and covers the period 1982–2007. Although this gridded global dataset is useful for validation of ESMs, its key limitations are also discussed in the literature (Jung et al., 2011). Wide geographical regions are not represented by measurement stations; for example, there is a lack of samples over Siberia, Africa, South America and tropical Asia compared with North America and Europe. Estimates of annual-mean upscaled ecosystem respiration have higher certainty than the anomalies and show approximately 5–10% underestimation. Additionally, the data have limitations in accounting for disturbances due to land use changes, given that unchanged land cover data from the International Geosphere-Biosphere Program (IGBP) satellite are used for all periods. This may introduce spurious trends into the GPP estimates from the FLUXNET-MTE project. The dataset does not provide estimates of  $R_a$ , but instead provides the summation of  $R_a$  and  $R_h$ . The geographical distribution of satellite-derived GPP from MODIS shows a high degree of consistency with that from in situ FLUXNET observations. Figure 2 compares the annual GPP distributions from MODIS and FLUXNET for the same period, 2000–2005. A notable difference between the two appears in the Amazon, where MODIS tends to underestimate the productivity significantly. In the remaining regions, MODIS tends to produce slight underestimates in the tropics and overestimates in the high latitudes when compared with FLUXNET. The annual GPP values from MODIS and FLUXNET are 108.76 GtC and 107.41 GtC, respectively, for the averaging period of 2000–2005, with a small difference that is no more than 1% of the total value. The pattern of differences did not change significantly even if the

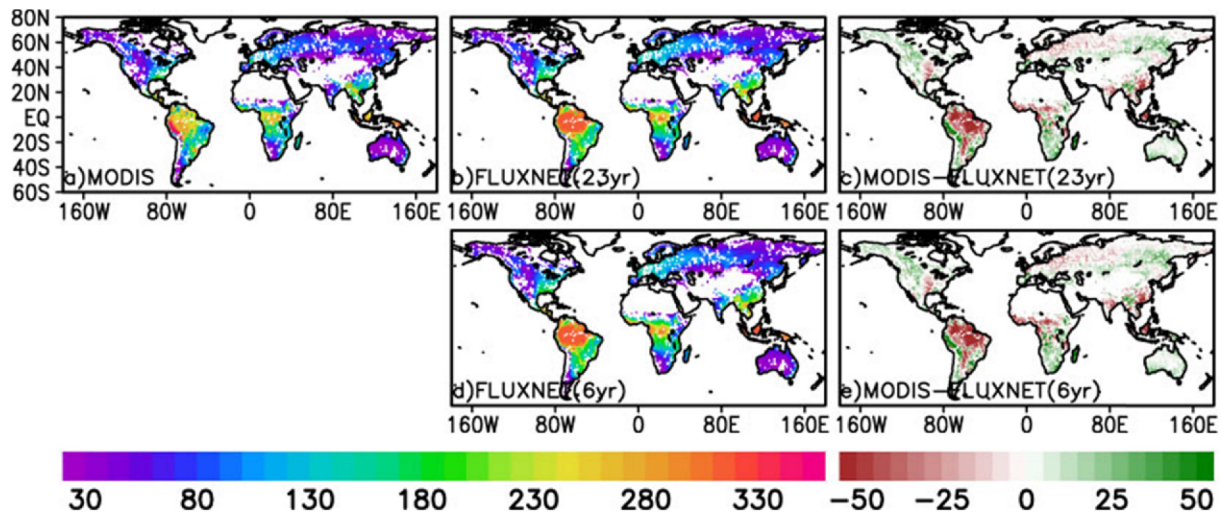


**Fig. 2.** Spatial distributions of annual-mean GPP from MODIS (upper left), FLUXNET (upper middle), and MODIS minus FLUXNET (upper right) averaged for 23 years (1983-2005). Bottom panels show the GPP from FLUXNET averaged for 6 years (2000-2005, bottom left), and its difference from MODIS averaged for 6 years (bottom right). The unit is  $\text{gC m}^{-2} \text{mon}^{-1}$ .

FLUXNET data were averaged over a longer period (1983-2005). In fact, the interannual variation did not modify the global-mean annual GPP value significantly when the reference period was extended to 1983-2005, which yielded a small reduction to  $106.55 \text{ GtC}$  using the FLUXNET data.

This study also used the observed surface air temperature and precipitation data from the Institute for Climate Impact Research based on the CRU (Climate Research Unit) meteorological dataset (Harris et al., 2014). In this data product, temperature and precipitation at stations worldwide were interpolated to a horizontal resolution of  $0.5^\circ \times 0.5^\circ$  (latitude  $\times$  longitude) covering the global land surface.

### b. Model data

Historical simulations performed using 10 ESMs were used in this study. Brief descriptions of these models is provided in Table 1. The historical simulations (that is, experiment 5.2 or the ESM historical 1850-2005 simulation; Taylor et al., 2012) were forced by gridded  $\text{CO}_2$  emissions data for fossil fuel consumption from Andres et al. (2011). While conventional  $\text{CO}_2$  concentration-driven runs have no vegetation feedback on atmospheric  $\text{CO}_2$ , these emissions-driven runs enable climate-carbon cycle feedbacks via changes in vegetation. Note that three models - GFDL-ESM2M, GFDL-ESM2G, and MPI-ESM LR - of them enabled the dynamic vegetation model in their historical simulations for 1850-2005, which model was able to consider dynamic change of PFT boundaries by climate conditions (Table 1). Hurtt et al. (2011) produced the land use change data, where the vegetation change was represented with the four basic land units (primary, and secondary vegetation, cropping, and pasture). Each ESM categorized the data from Hurtt et al. (2011) into their own PFTs and specified the vegetation change during the historical run. Atmospheric  $\text{CO}_2$

concentrations are simulated prognostically from the net budget of natural and anthropogenic carbon fluxes to and from the atmosphere. The simulation of GPP is directly controlled by the formulae representing photosynthesis in the models. As shown in Table 1, the parameterization of photosynthesis by vegetation is formulated similarly in the 10 ESMs. This parameterization is mostly based on Farquhar et al. (1980) for C3 plants in cold climates, with revisions for C4 plants in warm climates by Collatz et al. (1992). Leaf photosynthesis in CLM4 is proportional to the concentration of carbon dioxide in the atmosphere, as well as the temperature and moisture surrounding leaves. It adjusted the minimum rate among the light-use, water-use and carbon assimilation approaches in CLM4.

NPP is diagnosed in ESMs by subtracting  $R_a$  from GPP. Parameterizations for  $R_a$  are more diverse in formulation across the models compared to that of photosynthesis. Note that CESM1-BGC and NorESM-ME1 incorporate identical land surface models, in which the nitrogen cycle is allowed to limit plant assimilation for the parameterization of carbon fluxes by terrestrial vegetation, so called the interactive carbon-nitrogen (CN) cycle. Respiration is proportional to temperature and nitrogen concentration. The models without interactive nitrogen cycles diagnose nitrogen concentrations from the carbon concentration in each carbon pool, whereas the models with interactive nitrogen cycles predict the nitrogen concentrations. The only exception is MRI-ESM, which uses an empirical formula for estimating NPP based on Obata (2007). In the model, the monthly NPP is empirically derived from physical variables such as temperature and precipitation from the Miami model (Lieth, 1975; Friedling et al., 1995).

The model data were obtained from the Earth System Grid Federation (ESGF), an international network of distributed climate data servers (Williams et al., 2011). For the purposes of comparison, the model outputs, as well as the MODIS data,



**Table 1.** List of ESMs used in this study and their features.

Models	Modeling center	Horizontal resolution	ESM Reference	Land model	Photosynthesis	Autotrophic Respiration	Nitrogen Cycle	Dynamic Vegetation
1	BCC-CSM 1	Beijing Climate Center, China	$2.812^\circ \times 2.812^\circ$	Wu et al. (2013)	BCC-AVIM1	Farquhar et al. (1980)	Foley et al. (1996)	No
2	BCC-CSM 1M	Beijing Climate Center, China	$1.125^\circ \times 1.125^\circ$	Wu et al. (2013)	BCC-AVIM1	Farquhar et al. (1980) Collatz et al. (1992)	Foley et al. (1996)	No
3	CanESM2	Canadian Centre for Climate Modeling and Analysis, Canada	$2.812^\circ \times 2.812^\circ$	Arora et al. (2009)	CTEM	Farquhar et al. (1980) Collatz et al. (1992)	Ryan (1991)	No
4	CESM1-BGC	Community Earth System Model Contributors, NSF-DOE-NCAR, USA	$1.25^\circ \times 0.9^\circ$	Long et al. (2013)	CLM4	Farquhar et al. (1980) Collatz et al. (1992)	Foley et al. (1996)	No
5	GFDL-ESM2M	NOAA Geophysical Fluid Dynamics Laboratory, USA	$2.5^\circ \times 2^\circ$	Dunne et al. (2012)	LM3	Farquhar et al. (1980) Collatz et al. (1992)	Foley et al. (1996)	Yes
6	GFDL-ESM2G	NOAA Geophysical Fluid Dynamics Laboratory, USA	$2.5^\circ \times 2^\circ$	Dunne et al. (2012)	LM3	Farquhar et al. (1980) Collatz et al. (1992)	Ryan (1991)	Yes
7	MIROC-ESM	Japan Agency for Marine-Earth Science and Technology, Atmosphere and Ocean Research Institute, and National Institute for Environmental Studies, Japan	$2.812^\circ \times 2.812^\circ$	Watanabe et al. (2011)	MATSIRO+ SEIB-DGVM	Farquhar et al. (1980)	Ryan (1991)	No
8	MPI-ESM LR	Max Planck Institute for Meteorology, Germany	$2.812^\circ \times 2.812^\circ$	Giorgetta et al. (2013)	JSBACH	Farquhar et al. (1980)	Obata (2007)	Yes
9	MRI-ESM1	Meteorological Research Institute, Japan	$1.125^\circ \times 1.125^\circ$	Yukimoto et al. (2011)	HAL	Farquhar et al. (1980) Collatz et al. (1992)	Ryan (1991)	No
10	NorESM1-ME	Norwegian Climate Centre, Norway	$2.5^\circ \times 1.875^\circ$	Tjiputra et al. (2013)	CLM4	Farquhar et al. (1980) Collatz et al. (1992)	Foley et al. (1996)	No

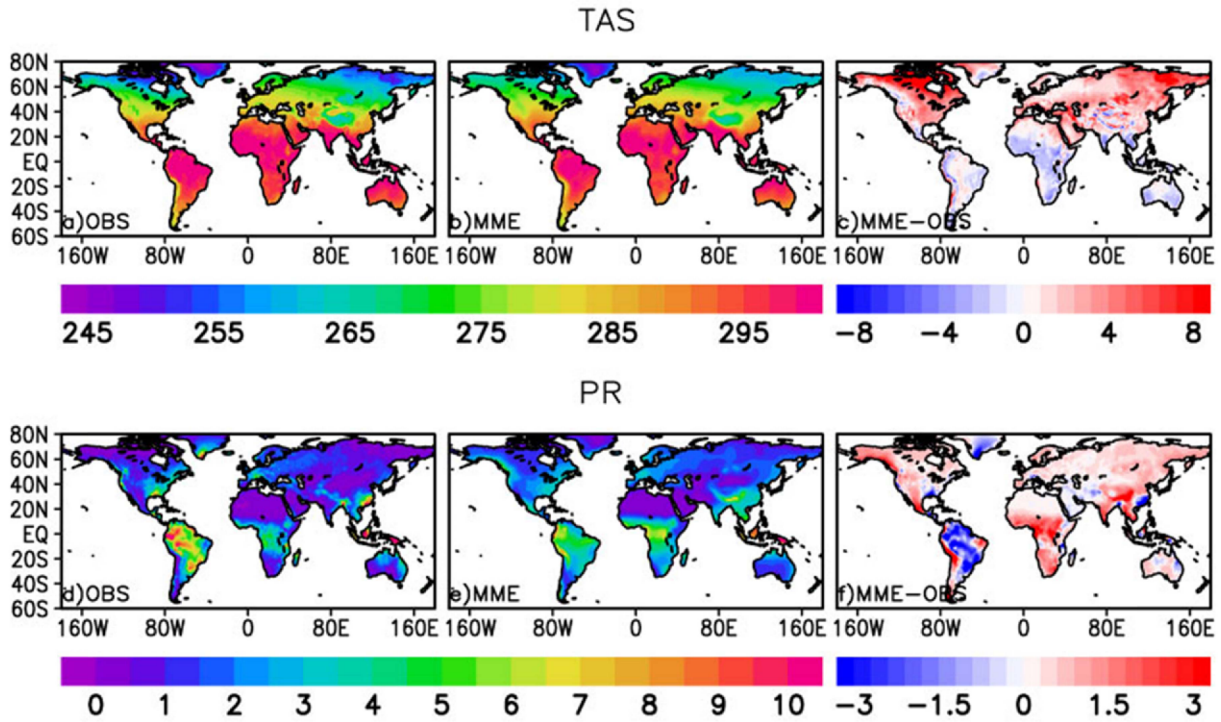


**Fig. 3.** Annual-mean surface air temperature (top panels, Unit: K) and precipitation (bottom panels,  $\text{mm d}^{-1}$ ) averaged for 2000-2005 from the CRU observations (left), and the multi-model ensemble (MME) mean (middle), and the model biases (MME minus CRU, right).

were interpolated onto the same  $1^\circ \times 1^\circ$  grid (latitude  $\times$  longitude).

### c. Analysis methods

In Section 3.3, CUE is diagnosed at the ecosystem level for the MODIS observations and the various ESM simulations. For simplicity, an identical distribution of vegetated surfaces based on to the MODIS classification (Fig. 1) was applied to both the observed and the simulated fluxes. This is because each model has their own vegetation classifications, which are not available from the CMIP5 data archive.

It is noted that the deficiency in the simulation of CUE by individual models is not only caused by deficiencies in the parameterization of carbon fluxes due to vegetation but also by differences in the classifications of PFTs, which are specified differently in each model. For example, LM3.0 in GFDL ESM2 M and ESM2G simulate 5 PFTs (i.e., 3 types of trees and 2 types of grasses), while NCAR and NorESM's CLM4.0 specifies the PFTs in much greater detail by including 17 different types (i.e., 8 types of trees, 3 types of shrubs, 3 types of grasses and 3 types of crops). Although referencing PFTs from the observations instead of using own PFTs in each model might not be a perfect comparison, it is still meaningful to identify the first order differences driven by parameterization method and the classification difference as well where the latter is regarded as the model bias too.

## 3. Results

### a. Systematic biases in the multi-model ensemble

Systematic biases in the ESM simulations are examined first by taking multi-model ensemble averages (MME) for simulated surface air temperature and precipitation, respectively (Fig. 3). Despite the realistic representation of annual-mean surface temperatures, MME exhibits systematic biases with significant hemispheric differences. Warm biases are seen in the Northern Hemisphere, particularly in northeastern Asia and North America, whereas there exists a cold bias in most of the Southern Hemisphere. MME generally shows wet biases in precipitation, except over South America. The individual model biases in temperature and precipitation show less variation across the models (See the supplementary Figs. S1 and S2). Wet biases seem to be consistent with cold biases in the tropical regions, where the deep convective rainfall tends to produce deep clouds that attenuate incoming solar radiation at the surface. The bias patterns of ESMs in surface temperature and precipitation obtained from this study are consistent with the validation results from Anav et al. (2013) using a slightly different collection of CMIP5 ESMs and for a longer validation period (1986-2005).

The global-mean values of GPP, NPP, and Ra are compared in Fig. 4. Note that spread of the simulations is large, particularly due to the outlier value produced by MRI-ESM1.

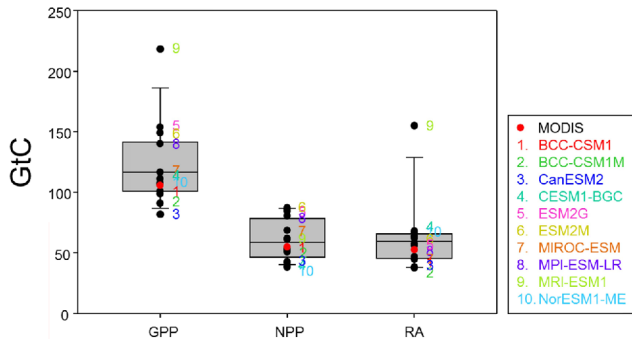


**Fig. 4.** Global-mean values of GPP, NPP and Ra from MODIS and CMIP5 ESMs. The values are the average over the land grids only with latitude weighting for the period of 2000 - 2005. Boxes are upper and lower quartile and median values are in the solid lines in the boxes.

MRI-ESM1 uses the empirical formulation for GPP and Ra. This aspect will be revisited in Section 3c where the simulation dependence on model formulation is discussed. The median value of GPP simulated by ESMs is centered slightly above the value from MODIS and is approximately 20% higher (+18 GtC). The median value of NPP is also overestimated by 10.2 GtC compared with the 52.1 GtC NPP from MODIS. The

median value of Ra is underestimated.

The annual GPP, NPP and Ra values from the MODIS observations and the MME are compared in Fig. 5. In MME, we exclude MRI-ESM1 as an outlier to avoid the overwhelming bias caused by it. The observed GPP values from MODIS are generally high in areas of EBF in tropical regions, such as Amazon, South Asia, and Central Africa, and in areas of DBF, such as those in Indochina, China, India, Europe and the southeastern part of North America. GPP is observed to be small in areas of SHR in Australia and in boreal regions of MF and GRA in northern Eurasia. GPP is close to zero over dry and non-vegetated surfaces, such as the Sahara Desert and central Australia. The MME of the ESMs tends to reproduce these geographical differences realistically, although the estimated magnitudes are too large over most of the globe except the Amazon region. Although Ra tends to be overestimated as well, MME shows a net positive bias in NPP in most terrestrial regions, suggesting that the MME should underestimate the observed trend of atmospheric CO<sub>2</sub> increase.

The bias patterns in GPP and NPP tend to reflect the impacts of simulated climate. The warm and wet bias in MME corresponds to the overestimation in GPP and NPP in the boreal region (c.f. Figs. 3c, 5c, and 5f), particularly in North America and the northeast Eurasia. In the low-latitudes, the GPP and

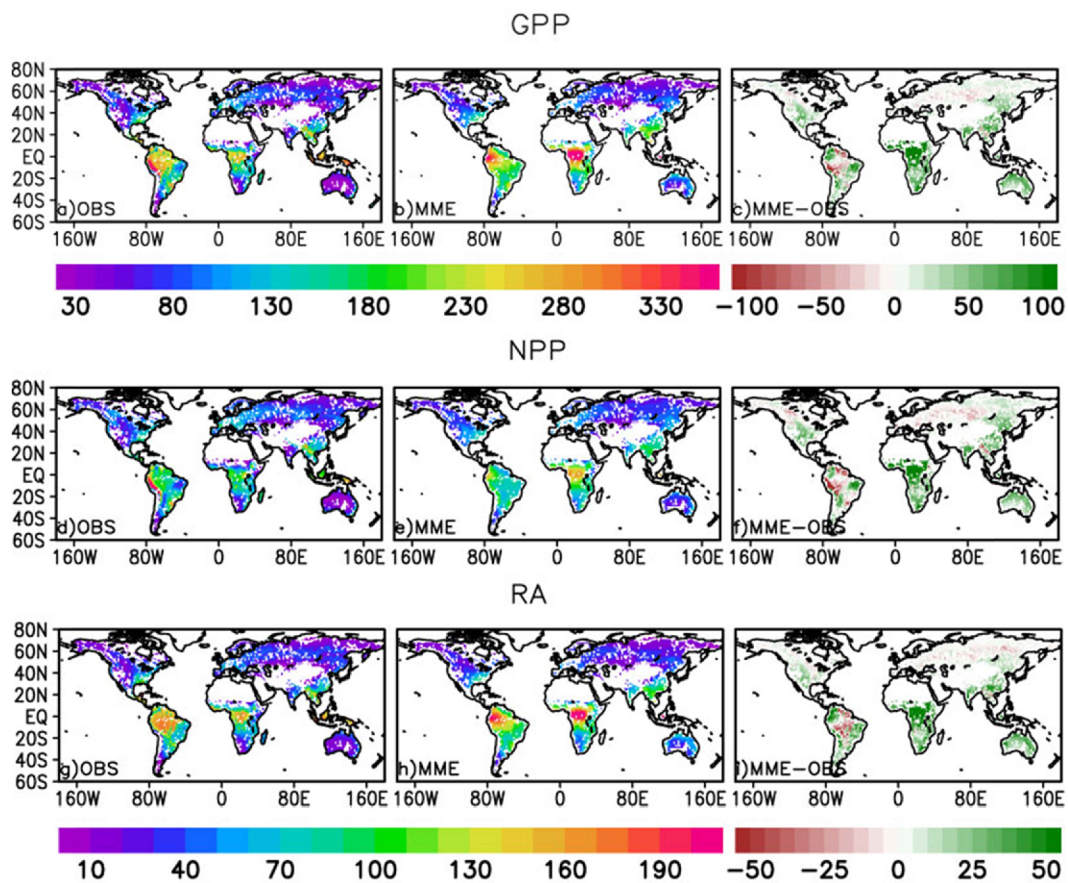


**Fig. 5.** Same as in Fig. 3 except GPP (top), NPP (middle), and Ra (bottom) from the MODIS observations and MME. MRI-ESM1 is excluded in MME as an outlier. See the text for detail. The unit is gC m<sup>2</sup> mon<sup>-1</sup>.

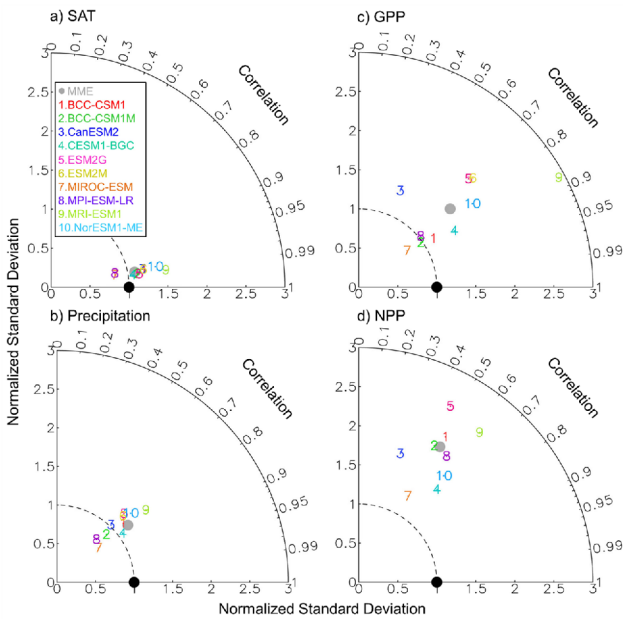


**Fig. 6.** Taylor diagram of CMIP5 ESMs for annual-mean distribution of (a) surface air temperature, (b) precipitation, (c) gross primary production (GPP) and (d) net primary production (NPP) with respect to the corresponding observations for 6 years (2000-2005). Only the vegetated grid points were included. The observed values are from CRU for temperature and precipitation are MODIS for GPP and NPP.

NPP biases in MME show more dependence on precipitation (c.f. Figs. 3f, 5c, and 5f). MME exhibits wet biases over the regions where GPP and NPP show positive biases, whereas the negative biases in GPP and NPP in Amazon correspond to the dry bias. MME exhibits overall cold bias in most of the tropics and the Southern Hemisphere, which has less relationship with the GPP and NPP biases. This result is consistent with the previous studies. Nemani et al (2003) and Piao et al. (2009) suggested that temperature, water availability and radiation are related with the terrestrial primary production based on the observational data. They showed that temperature is a major contributor in the Northern Hemisphere high latitudes, while in the tropics and sub-tropics the water availability impacts more.

The formulations of GPP and Ra are closely related to temperature and precipitation (Rahman et al., 2005; Yang et al., 2006), and the model biases in those carbon fluxes might be driven both by systematic biases in climate conditions such as temperature and precipitation and the uncertainty in the parameterization formulations themselves. The Taylor diagram is a common and useful measure for simulated spatial distributions that calculates spatial correlation coefficients between observed and simulated values and the normalized standard deviation of simulated values from the global mean over the whole domain of comparison. Fig. 6a and 6b show Taylor diagrams (Taylor, 2001) for the annual mean surface air temperature and precipitation, respectively. The MME simulation of temperature by the CMIP5 ESMs is quite close to the CRU

observations. The spatial correlations are greater than 0.95 in all models. The normalized standard deviations are within the range of 0.81 to 1.50, which is relatively small compared with other simulated variables. The Taylor diagram of precipitation shows less accuracy and more model spread than that of SATs. The spatial correlation of the MME is approximately 0.76; the MME also shows higher normalized standard deviations compared with temperature, suggesting that current ESMs exhibit relatively larger discrepancies in precipitation and the terrestrial water cycle. Spatial patterns of GPP simulated by the ESMs (Fig. 6c) show even larger systematic biases with lower spatial correlations and larger spatial changes (i.e., higher normalized standard deviations) than the observed values. Model spread becomes much larger than that of temperature and precipitation. The simulated pattern correlations from the ESMs are lowest for NPP (Fig. 6d). The correlation for the MME is slightly higher than 0.5. The models also exhibit much higher spatial variation than the observed values for both GPP and NPP.

The much larger spread in GPP and NPP simulated by the ESMs compared to that in temperature and precipitation suggests that there should be much larger uncertainty in the parameterization of terrestrial carbon cycle in the current ESMs. Biases and model spread are even larger in NPP compared with GPP, implying that the simulation uncertainty is much larger when the photosynthesis and the respiration are combined. The performance of the MME in terms of GPP and NPP is not necessarily higher than that of the individual models in this case, due to the presence of persistent and large deficiencies in the individual models. Individual models have the different bias patterns of GPP and NPP. Therefore, MME shows the good simulation skills for spatial distributions of GPP and NPP in CMIP5-ESMs.

**b. Model dependences**

The simulation of annual GPP values shows significant model dependence as shown in Fig. 4. MRI-ESM1 shows the largest value among the models. The three models, ESM2G, ESM2 M, and MPI-ESM-LR, simulate relatively larger values of GPP than the rest of the models. As the simulation of Ra shows relatively small model dependence, models that simulate larger GPP values tend to produce larger NPP in general. MRI-ESM1 is an exception, and the simulated GPP of this model is significantly reduced by its large Ra, leading to an NPP value close to the median value. The two models, CESM1-BGC and NorESM1-ME, that share the same land surface model simulate the smallest NPP values, which is a significant underestimation relative to the MODIS estimate.

To examine further what causes the global bias in carbon fluxes, the spatial distribution of the GPP bias pattern in carbon fluxes simulated using each model is compared in Fig. 7. Each model exhibits its own systematic biases. MRI-ESM1 shows a significant positive bias in most vegetated regions, which is particularly pronounced in tropical rainforests. The



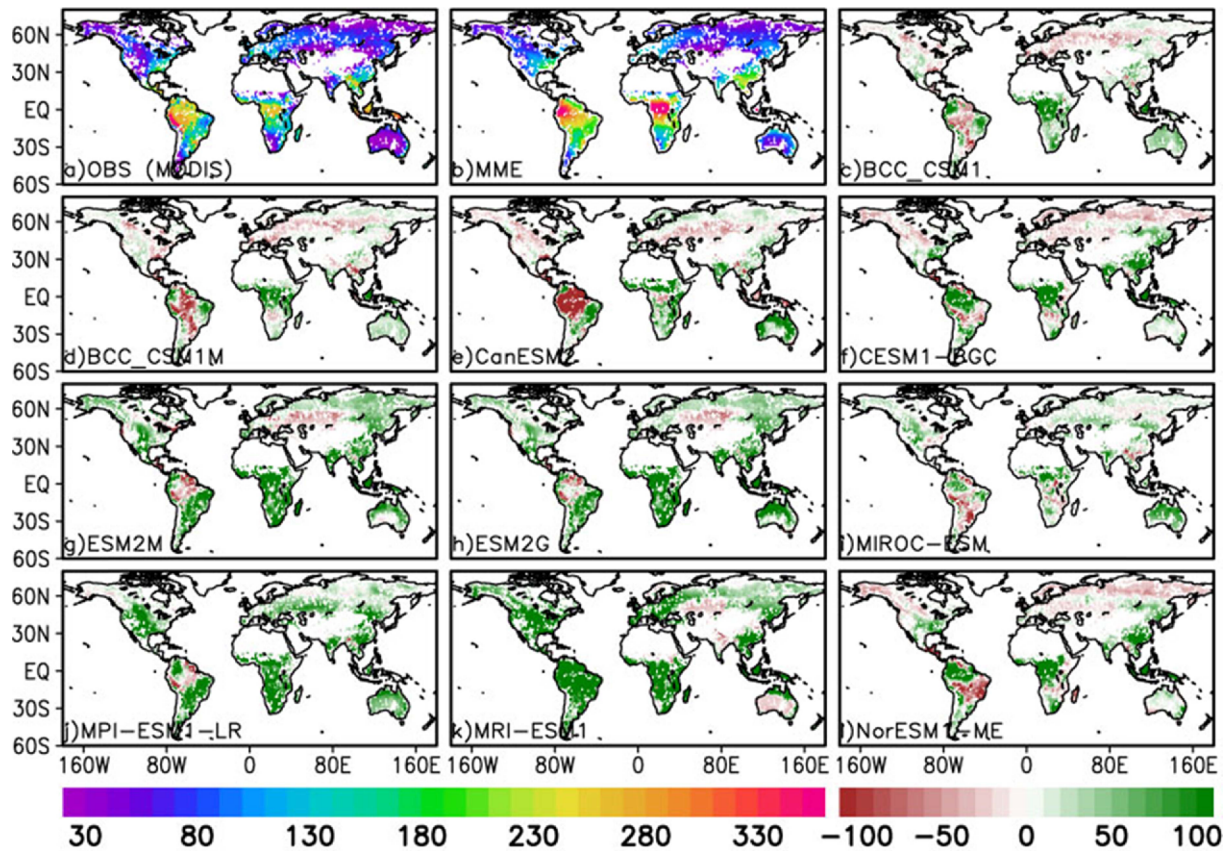


**Fig. 7.** Spatial distribution of annual GPP from the MODIS observation (top left), MME (top middle) and the simulation bias in each model (model minus MODIS). The unit is  $\text{gC m}^2 \text{mon}^{-1}$ .

group of models with higher global-mean GPP values in Fig. 4 (i.e., MPI-ESM1-LR, ESM2 M, and ESM2G) shows GPP bias patterns that are remarkably similar to each other. GPP is overestimated in most regions in these models except for the upper inland region of the Amazon. The rest of the models show mixed spatial patterns of positive and negative biases. The large negative GPP bias in part of the Amazon is primarily responsible for the lowest global-mean GPP values, which are simulated by CanESM2 and BCC\_CSM1 M. The negative bias is clear in the boreal high-latitude regions above  $40^\circ\text{N}$  in the CESM1-BGC and NorESM1-ME models. The systematic biases in the models reflect the uncertainties in the parameterized carbon cycles, as well as in the simulated climates. Mao et al. (2012) suggested that simulated GPP using offline CLM4 experiment with observed forcing showed similar biases of GPP spatial distribution as like CESM1-BGC in CMIP5 (positive over tropics and negative over high latitude in northern hemisphere). It suggests consistently that the bias in climate simulated by ESMs is not the single major reason for the biases in GPP and NPP simulations.

Most models simulate larger production in the tropics, due to abundant rainfall and high temperatures, and smaller production in high latitudes due to less precipitation and low temperatures. As GPP is much larger in magnitude than Ra,

the NPP bias pattern in each model is mostly dominated by that of GPP rather than Ra, leading to consistent patterns (c.f., Fig. 7 and Fig. 8). The two GFDL models implemented with the same LM3 land surface model (i.e., ESM2M and ESM2G) and the other two models that use CLM4 (CESM1-BGC and NorESM1-ME) show NPP biases with opposite signs in the boreal regions above  $40^\circ\text{N}$ , highlighting significant model differences in parameterizations of carbon fluxes due to vegetation.

### c. Carbon use efficiency

The bias patterns of GPP and NPP simulated by the various ESMs presented in Fig. 7 and 8 are the result of complicated feedbacks between the carbon cycle (mostly by terrestrial vegetation) and climate. As the magnitude of the bias is also a function of biomass, this study further compared carbon use efficiency by dividing NPP by GPP. This normalized carbon flux ratio can highlight the difference among simulations driven by parameterization differences in terrestrial carbon fluxes by vegetation. Moreover, CUE is one of good indicator for measurement of carbon cycle over terrestrial region. The spatial pattern of CUE obtained by MODIS shows significant variations (Fig. 9). In MODIS, most tropical areas with high



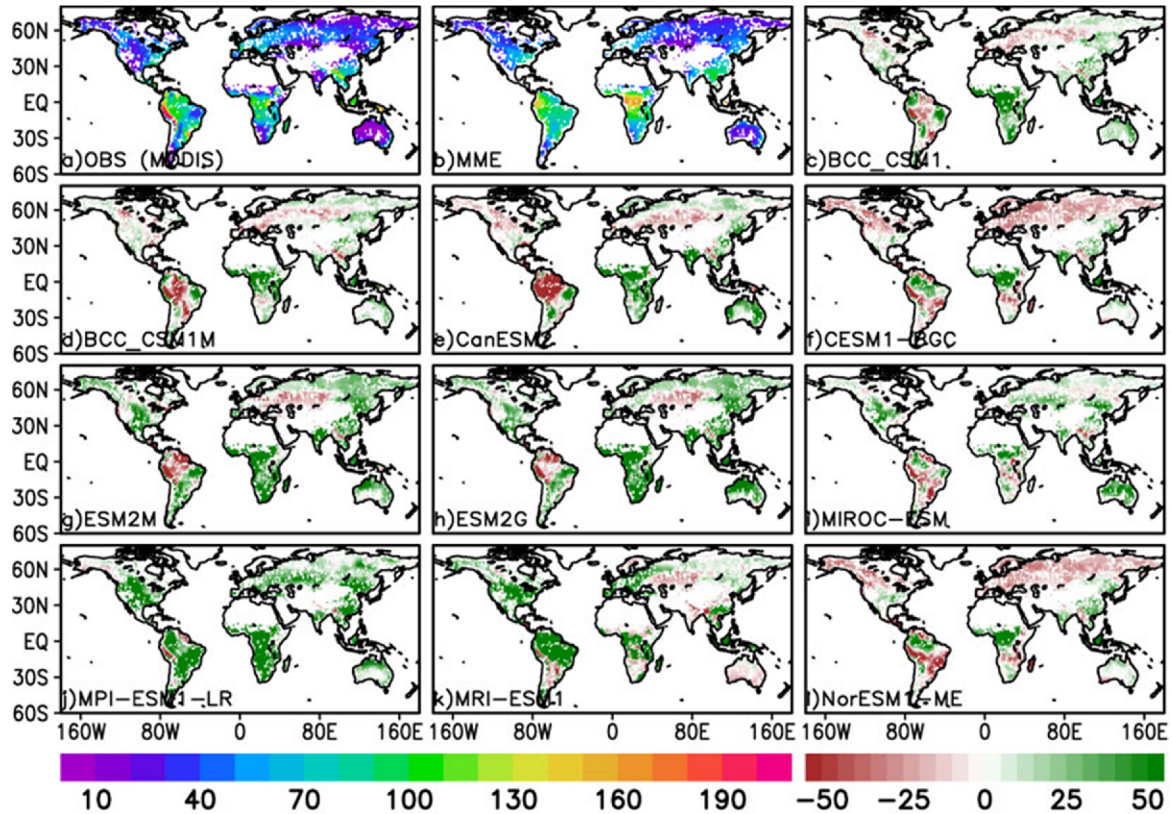


**Fig. 8.** Spatial distribution of annual NPP from the MODIS observation (top left), MME (top middle) and the simulation bias in each model (model minus MODIS). The unit is  $\text{gC m}^{-2} \text{mon}^{-1}$ .

GPP values generally show low CUE values below 0.4, particularly over the Amazon, central Africa and Southeast Asia. In contrast, CUE is in general greater than 0.5 over wide areas in high latitudes and a few low-latitude, high-elevation regions. The spatial distribution of CUE apparently depends on climate conditions such as precipitation and temperature in that regions with large amounts precipitation and warm climates show low CUE values, while regions experiencing dry and cold climates show high CUE values. Overall, the MME of 10 ESMs tends to reproduce the observed distribution from MODIS reasonably well. However, the MME values are lower than the observed values in most regions, which can largely be attributed to the underestimation of CUE values by MRI-ESM1. The bias pattern of CUE differs strongly among the models. Note that the bias pattern of CUE tends to characterize the parameterization differences in the terrestrial carbon fluxes used in the ESMs. The bias patterns of CUE are almost identical to each other for models that share the same land surface model, such as BCC-CSM1 and BCC-CMS1M, and ESM2M and ESM2G, and CESM1-BGC and NorESM1-ME, respectively. The two BCC models tend to overestimate CUE in Eurasia, North America, and Africa, while they produce underestimates in Australia and South America. CanESM2 shows a similar pattern as the two BCC models. MPI-ESM1-LR shows a similar bias structure except in that it produces

overestimates in South America. CESM1-BGC, NorESM1-ME, and MRI-ESM1 exhibit an underestimation of CUE over most terrestrial regions.

The model dependence is depicted better by the zonal mean CUE distribution (Fig. 10). The observed CUE values show a clear latitudinal dependence and generally increases with latitude. The zonal mean of CUE from MODIS ranges from 0.3 to 0.7, with a global average of 0.49. It indicates that the biomass in high latitudes tends to take up atmospheric carbon more efficiently compared with that in tropics. Even though the model spread is larger, the zonal mean MME is able to reproduce the observed relationship between CUE and latitude. Some models, such as CESM1-BGC, NorESM1-ME and MRI-ESM1, are notably different from the other models, as well as from MODIS, and simulate low values, particularly at middle to high latitudes. These results are consistent with those in Shao et al. (2013). They suggested that respiration decreases more rapidly than production in response to latitudinal decreases in mean temperature in all models except NorESM1-ME and CESM1-BGC. The reason for the underestimation of CUE in the two models are caused by their low estimates of NPP. Using the same data from MODIS, Zhang et al. (2009) suggested that there exists a clear relationship between CUE and climate conditions, such as surface air temperature and precipitation, that are critical for biomass growth.

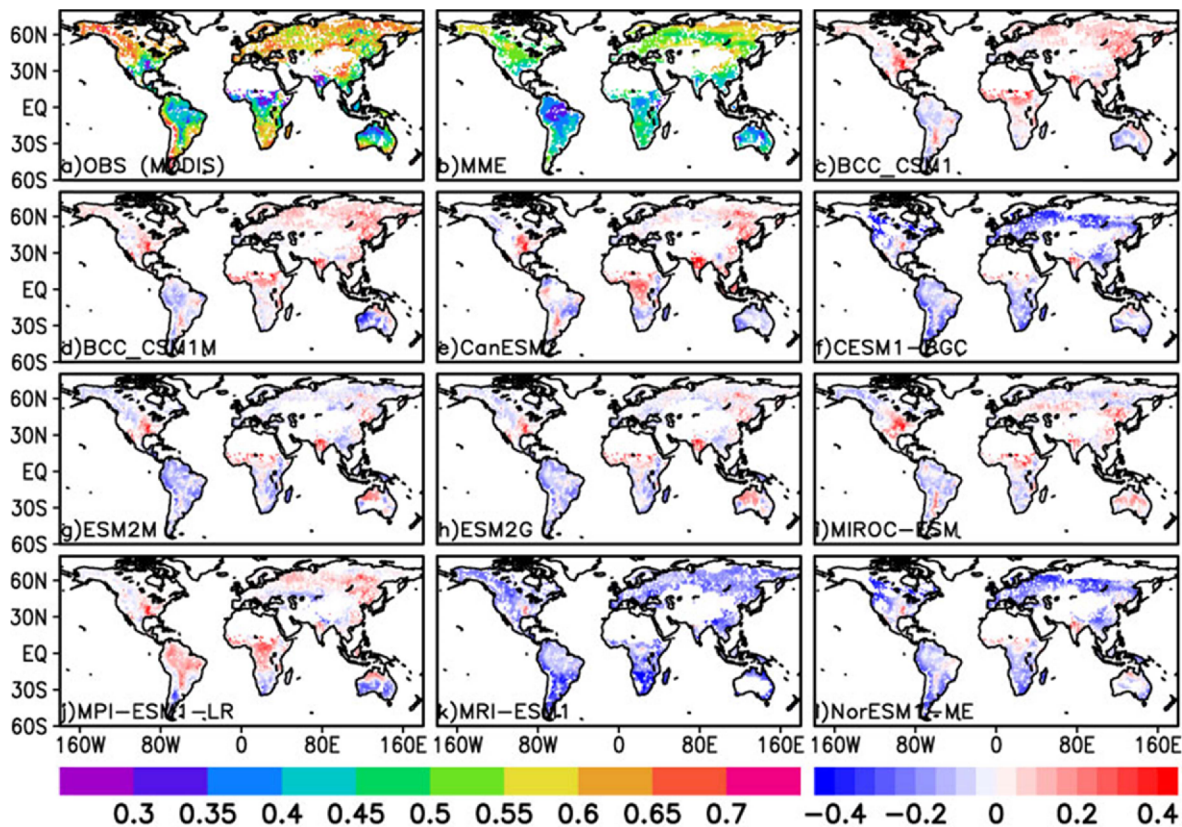


**Fig. 9.** Spatial distribution of annual CUE from the MODIS observation (top left), MME (top middle) and the simulation bias in each model (model minus MODIS). CUE is a positively-defined ratio as NPP divided by GPP and less than or equal to 1.

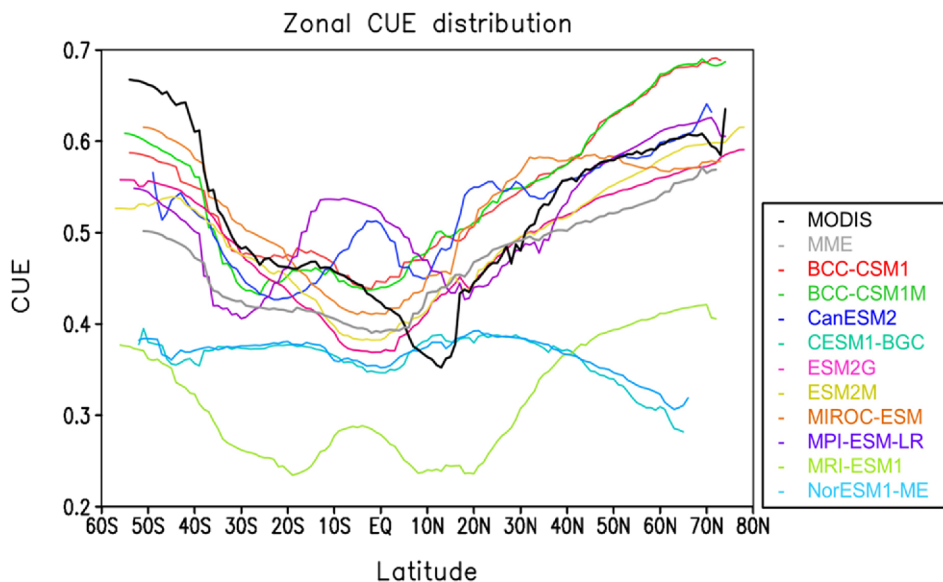


**Fig. 10.** The zonal mean CUE from MODIS (black), MME (grey), and 10 ESMs.

Figure 11 compares the relationship from MODIS with the model simulations. The observed CUE from MODIS is more influenced by temperature than precipitation, as is particularly

clear in dry regions with precipitation below  $50 \text{ mm yr}^{-1}$ . In general, the observed CUE decreases with increasing temperature. Moreover, observed CUE values show the sensitivity



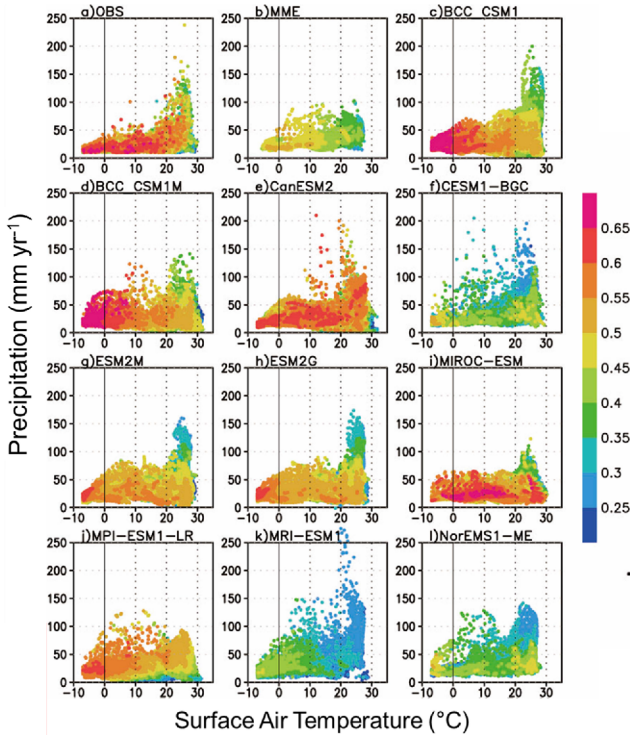


**Fig. 11.** Scatter plot of CUE with the variation of surface air temperature (x-axis) and precipitation (y-axis). Color indicates CUE.

of CUE to precipitation in the tropics, where plant growth is more sensitive to precipitation compared with high latitudes. The MME basically follows this temperature sensitivity, although it tends to underestimate CUE. It is caused by the overestimation of  $R_a$  in most models compared with the MODIS estimates (See the supplementary Fig. S3). Individual models show their own deficiencies. For example, the GFDL models (ESM2 M and ESM2G) tend to overestimate the sensitivity of CUE to precipitation in tropical regions compared with MODIS. It indicates that the gradients in CUE with temperature in the GFDL models are weaker than those in MODIS. In contrast, the models based on CLM4.0, such as CESM1-BGC, NorESM1-ME and MRI-ESM1, show a weaker sensitivity of CUE to both temperature and precipitation than the other models. This result might be caused by other limiting and trigger processes, such as nitrogen limitation, which are larger than the sensitivity to temperature and precipitation. This large divergence in the model sensitivity of CUE to temperature and precipitation induces differences in the atmospheric  $CO_2$  concentrations in the future among the full coupled ESMs.

Figure 12 compares the observed values and differences among simulations in terms of CUE depending on the dominant PFTs according to the classification in Fig. 1. In the MODIS observations, the CUE values over broadleaf forests (DBF and EBF) are generally lower than over needleleaf forests which usually represents to gymnosperms (DNF and ENF), implying that dense forests tend to not only take up

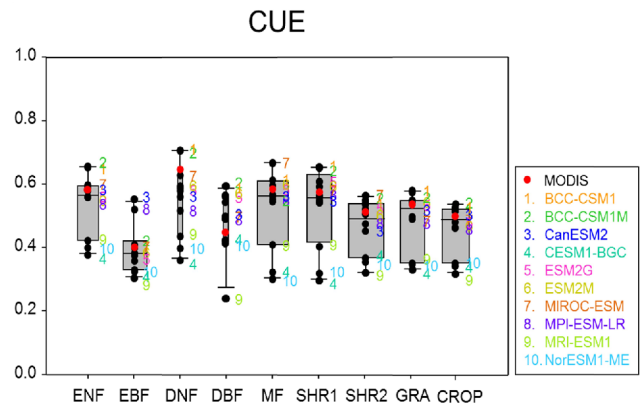


**Fig. 12.** CUE averaged for each PFT. The box widths are proportional to the root mean square of number of grids. The coefficients of proportionality box widths in each PFTs are: ENF (0.80), EBF (0.48), DNF (0.12), DBF (0.11), MF (1.25), SHR1 (0.91), SHR2 (1.78), GRA (0.70) and CROP (0.73).

large amounts of atmospheric carbon for photosynthesis but also release large amounts of carbon to the atmosphere through respiration. In this regard, the efficiency of carbon uptake by the broadleaf forests is smaller than that of needleleaf forests.

The observed variations in CUE depending on the PFTs are reproduced realistically by the MME. The differences between MODIS and the MME is large in areas of DNF and DBF, but those vegetation types occupy relatively small fractions of the vegetated surface. The model spread is large, regardless of plant function types. This is primarily due to the low CUE values produced by three of the models, CESM1-BGC, MRI-ESM1 and NorESM1-ME, for all of the plant function types. These three ESMs have their own unique formulations in parameterizing terrestrial carbon fluxes. In the case of MRI-ESM1, it determines the monthly  $R_a$  empirically based on a function of the surface air temperature and precipitation (Obata, 2007). The simulated NPP in MRI-ESM1 is the residual term between GPP and  $R_a$  that is evidently different from that of the other ESMs. The two CLM 4.0-based models, CESM1-BGC and NorESM1-ME, include coupled carbon and nitrogen (CN) cycles, which seems to lead to dramatic differences in CUE compared with the other models that do not represent interactions between the carbon and nitrogen cycles. Inclusion of the nitrogen cycle in the models tends to constrain the amount of carbon uptake in vegetated land surface (Zaehle et al., 2014; Friedlingstein et al., 2014) and produces higher simulated growth respiration than in other models (Shao et al., 2013).

To examine the impact of the CN cycle in the model further, this study conducted two additional sensitivity experiments using CESM1-BGC, one with interactive carbon-nitrogen cycle (CN) and the other with no nitrogen cycle (Only C). The Only C experiment assumes the saturation of nitrogen nutrients in the soil, and it is not limiting the plant assimilation and the carbon cycle. Both runs were integrated for 156 years (1850-

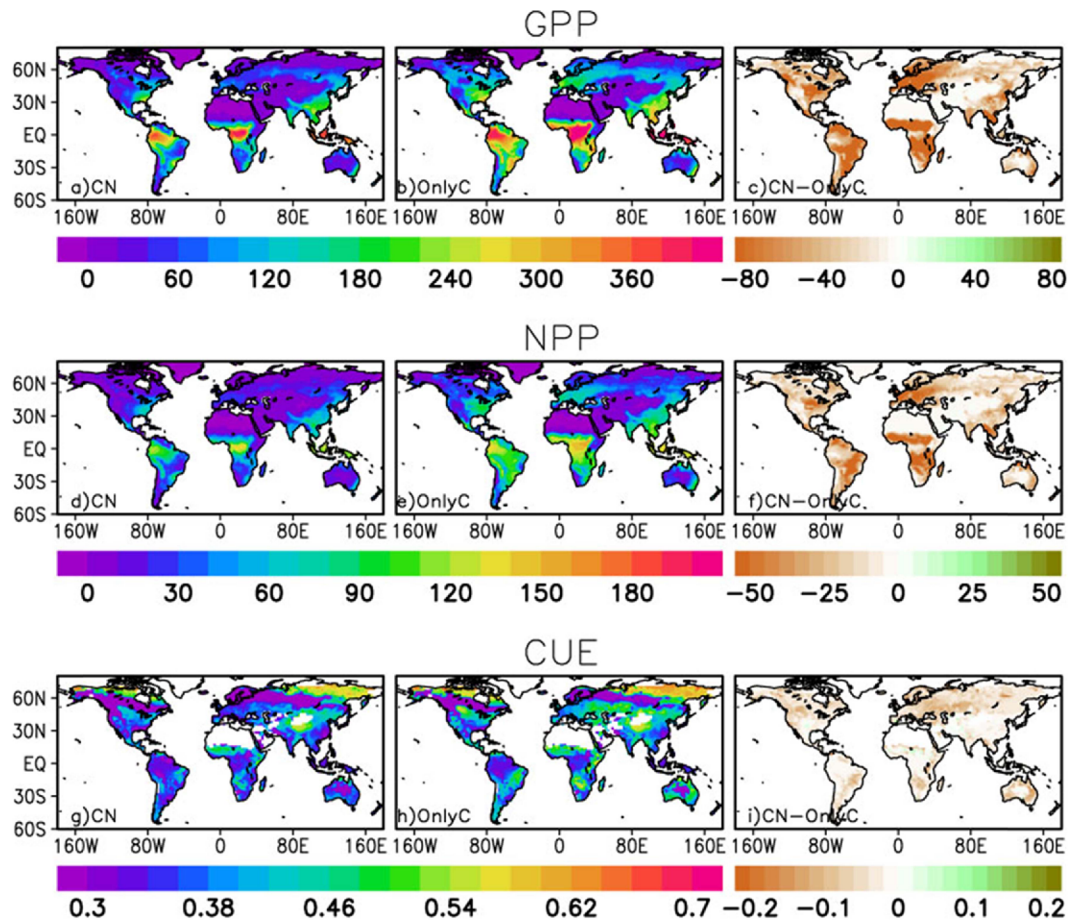


**Fig. 13.** Spatial distributions of annual GPP, NPP and CUE and their differences from the interactive carbon-nitrogen cycle simulation (CN) and the run with no nitrogen cycle (Only C) by CESM-BGC. The units of GPP and NPP are  $\text{gC m}^{-2} \text{mon}^{-1}$ . CUE is a positively-defined ratio as NPP divided by GPP and less than or equal to 1.

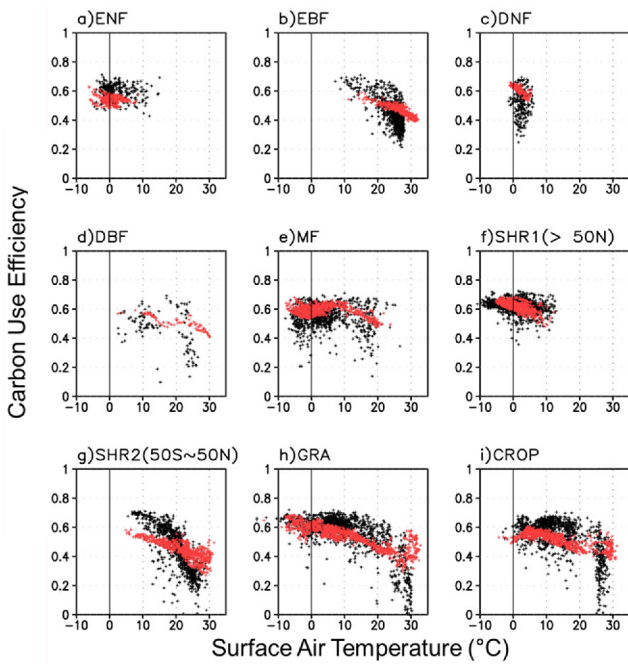
2005) from the initial states obtained from the long-term equilibrium run driven by prehistorical forcing. Atmospheric initial  $\text{CO}_2$  concentration was 273 ppm. Other historical changes such as in land use and land cover, anthropogenic emission, and atmospheric nitrogen deposition were specified according to the CMIP5 experimental design. The last 30 years were analyzed in this study.

Figure 13 shows that CN tends to decrease GPP in most of areas compared with Only C, which suggests that the implementation of nitrogen cycle in this model reduces the amount of carbon uptake by vegetation drastically as a limiting factor. Accordingly, NPP also tends to decrease in most of the regions at the decrease of GPP. It is interesting to see that CUE decrease is particularly significant in mid- to high-latitudes rather than in the tropics. This result is quite consistent with the simulation difference between the CN models (CESM1-BGC and NorESM1-ME) and the rest of ESMs (e.g., the zonal mean CUE shown in Fig. 10).

This study further compares the observed and the MME-simulated CUE sensitivity to the surface temperature for each plant function type (Fig. 14). The MODIS observations show

more scatter in CUE values for a given temperature, suggesting that the natural carbon cycle is not simply determined by temperature, but is also controlled by other factors. In most PFTs, the observed CUE is maintained close to or even higher than 0.6, particularly in low canopy plants such as SHR, CROP and GRA, for surface temperatures lower than  $10^\circ\text{C}$ . CUE tends to decrease significantly at temperatures higher than  $10^\circ\text{C}$ . This observed feature may be interpreted based on the ecological significance of the resistance to low temperatures by plants (Allen et al., 2010). Low temperatures tend to reduce biosynthetic production by plants and can even disturb vital functions to cause permanent injuries and death. The survival capacity of plants tries to make its metabolic processes continue to function under low temperature stresses and using its cold resistance (Larcher and Mair, 1968). It suggests that the CUE values of vegetation may be lowered in favorable environmental conditions, such as warm temperatures and abundant precipitation, as there is plenty of production and plant growth. Vegetation experiencing cold temperatures and insufficient precipitation adapts to survive by increasing CUE.

In contrast, even though the multi-model ensemble average



**Fig. 14.** Scatter plots of CUE (y-axis) as a function of temperature (x-axis). Each panel shows the plot for different PFT. Satellite-derived values from MODIS are presented with black dots and the multi-model ensemble (MME) average of 9 CMIP5 ESMs except for MRI-ESM1 are with red dots. MRI-ESM1 is excluded in MME as an outlier. See the text for detail.

is taken for the various ESMs, the simulated CUE variation shows a clearer change with temperature, suggesting that the parameterization of the terrestrial carbon cycle in current ESMs depends too much on temperature conditions. A decreasing trend is clear in the MME regardless of PFTs in response to an increase in temperature. From the MME simulation results, CUE values in all PFTs shows a clear linear change in response to temperature variation. This implies that the current models do not adequately consider the observed ecological resistance to temperature, and the balance between respiration and production in the models is more simplified than the observations.

In fact, the parameterizations of most land surface models are based on conceptual leaf-level formulations, such as those used in the calculation of biochemical photosynthesis processes and the dependence of  $\text{CO}_2$  exchange on stomatal conductance, which use temperature and soil moisture explicitly in their formulations. The comparison results in this study suggest that the models might need to consider ecosystem-level parameterizations which simulate carbon and nitrogen fluxes and vegetation and soil pools and are estimated at a long (e.g., monthly) time step based on spatially explicit information on climate, ecosystem type, soil type, and elevation (Zhu and Zhuang, 2015) to reflect the nonlinear relationship for the interaction between climate condition and vegetation.

It is noted that the soil moisture is also an important factor to affect vegetation production and respiration. Knapp et al.

(1993) investigated that the relationship between the soil water content and NPP is linear ( $R^2 = 0.66$ ). Shao et al. (2013) showed soil moisture is positively correlated with carbon fluxes in the current ESMs, although the relationship shows a large spread across the models. In our analysis (not shown), the CMIP5 ESMs show a similar and coherent bias patterns in annual-mean soil moisture simulation, with less resemblance to the bias patterns of annual GPP or Ra. This suggests, even though the soil moisture is one of the important factors in terrestrial carbon flux, the biases in GPP and Ra are affected more dominantly by model parameterizations.

#### 4. Summary and concluding remarks

The simulations of climate and the terrestrial carbon cycle have been examined by comparing surface temperatures and precipitation, as well as GPP, Ra, and NPP values, simulated by 10 different CMIP5 ESMs with the CRU surface observational data for climate-related variables and the MODIS satellite estimates for the carbon cycle over 6 years (2000-2005).

Despite the systematic biases with significant hemispheric differences, the spatial distributions of temperature and precipitation, which are closely related to biogeochemical variables (Rahman et al., 2005; Yang et al., 2006), are relatively similar when compared with observations. More model discrepancies appeared in the simulation of the carbon cycle, which reflects overestimation of GPP over most of the globe. The terrestrial carbon fluxes simulated by the ESMs are diverse, and the models exhibit large spread, even though the multi-model ensemble mean (MME) shows strong resemblance in terms of its spatial distribution to the observed pattern by cancelling out the systematic biases in each model. The results show that the biases of terrestrial carbon fluxes are due less to the bias in the spatial distribution of climate conditions but more to the larger uncertainty in their parameterizations.

We also analyzed carbon use efficiency (CUE) by dividing NPP by GPP, which is a physiological parameter defined as the proportion of carbon acquisition (e.g., GPP) to vegetation growth (NPP). Actually, the MODIS gridded data are not perfect observation data. Even though, MODIS GPP and NPP are based on the light use model with satellite forcing data. It is best and only one data to evaluate global distribution of CUE in ESMs. For evaluation of MODIS data compared with site based observation data, we compared carbon use efficiency (CUE) from our studies and previous studies which are site-based observation data in Table S1. DNF is highest CUE values in our study and all previous studies. In addition, the plants with short canopy height (SHR, GRA and CROP) are around 0.5 and needleleaf forest (ENF, DNF) is relatively higher than other PFTs in all studies. Therefore, MODIS satellite data is reasonable to use evaluation of gridded ESMs. Analyzing CUE help us to understand the carbon storage in simulated terrestrial ecosystem in ESMs. At first, the spatial distribution of observed CUE from space (e.g., MODIS)



depends on climate condition such as precipitation and temperature. For example, the regions of large precipitation and warm climate show low CUE, while the regions of dry and cold climate show high CUE. It indicates that CUE at the regions with warm temperature and abundant precipitation could be lowered as there is a plenty of production and plant growth. The vegetation in cold temperature and insufficient precipitation adapts to the environmental condition for survival by increasing CUE.

In contrast with MODIS, we found clear difference of CUE between ESMS. The bias pattern of two ESMS from BCC showed the hemispheric contrast to positive in NH and negative in SH. The strong negative bias of CUE over southern hemisphere is shown in GFDL's models. The CUE in ESMS based on CLM4 (e.g., CESM-BGC and NorESM-ME) are significantly underestimated globally. This large uncertainty of CUE in individual models is influenced by biogeochemical parameterization of land surface model. In the MME, the spatial distribution of CUE is reasonably simulated. However, Strong negative bias is found over Amazon. It is caused that unbalanced ratio of GPP and Ra in the terrestrial carbon fluxes over tropical forest such as evergreen broadleaf forest the most models. The inverse relationship between temperature and CUE is reasonably simulated in the MME over dry regions. Generally, Ra is more sensitive to temperature than GPP in the real world over a certain range of temperatures (Woodwell et al., 1990; Ryan, 1991; Piao et al., 2010). It means that the sensitivity of temperature to photosynthesis is weaker than that of respiration (Arnone III and Körner, 1997; Enquist et al., 2007). Actually, the sensitivity of CUE is not only function of temperature (Tucker et al., 2013) but also nitrogen availability (Zha et al., 2013). However, most ESMS in CMIP5 don't consider nitrogen cycle except CESM-BGC and NorESM. Moreover, ESMS adapted nitrogen cycle are not perfect (e.g., nitrogen fluxes and amounts are too much dependence onto carbon fluxes and amount in the models). It might lead non-linearity and complex relationship between CUE and temperature in the real world.

The CUE variation depending to the PFTs, MME is realistically reproduced in every PFTs. The model spread is large. It indicates a wide spread due to the different PFTs in

each land models and systematic bias such as failure of PFT description in land models. The observed CUE values show a reasonable degree of non-linearity in terms of its response to temperature. In contrast, the stronger sensitivity of CUE to temperature increases in the MME is reflected by the systematic biases of simulated biogeochemical processes which depends on temperature conditions strongly in every PFTs.

However, most of the advanced ESMS have adopted leaf-scale biogeochemistry which involves parameterizations of photosynthesis and respiration based on small spatio-temporal scales that depend on laboratory experiments and limited in situ studies. It makes up one of the major uncertainties of carbon cycle processes in future climate change simulations from recent advanced ESMS. Atkin et al. (2008) suggested that most biogeochemical models are adjusted and incomplete parameterizations of biogeochemical processes. Due to the lack of observational data, many biogeochemical studies have focused on the total amount of primary production and respiration. Therefore, understanding and evaluating the global-scale ecosystem is challenging, based on the leaf scale biogeochemical parameterization used in the models. This leaf-level parameterization for biogeochemical processes is insufficient for long-term simulations (Zaehle et al., 2014). For development of terrestrial parameterization of global-scale ecosystem, more fine spatial and temporal in-situ observation data are necessary. For realistic long-term simulations, such as climate change experiments including the carbon cycle and feedback processes, parameterizations representing idealized and generalized ecosystem-level processes are needed, rather than site-specific and leaf-level processes.

**Acknowledgements.** This study is supported Basic Science Research Program through the National Research Foundation of Korea (NRF), funded by the Ministry of Education, Science and Technology (2012M1A2A2671851) and the Supercomputing Center/Korea Institute of Science and Technology Information with supercomputing resources including technical support (KSC-2015-C3-035).

**Edited by:** Soon-Il An

### Supplementary Figures and Tables

**Table S1.** Comparison of averaged CUE for each PFTs.

	This study	De Lucia et al. (2007)	Amthor (2000)	Choudhury (2000)	Zhang et al. (2009)	Average (STD)
ENF	0.59	0.41	0.61	-	0.56	0.54 (0.09)
EBF	0.41	0.32	0.54	0.42	0.32	0.40 (0.09)
DNF	0.63	0.59	0.76	-	0.59	0.64 (0.08)
DBF	0.42	0.46	0.67	-	0.51	0.52 (0.11)
MF	0.60	0.45	-	-	0.41	0.49 (0.10)
SHR	0.54	-	0.50	0.45	0.52	0.50 (0.04)
GRA	0.54	-	0.49	0.52	0.51	0.51 (0.02)
CROP	0.52	-	0.45	0.56	0.52	0.51 (0.05)

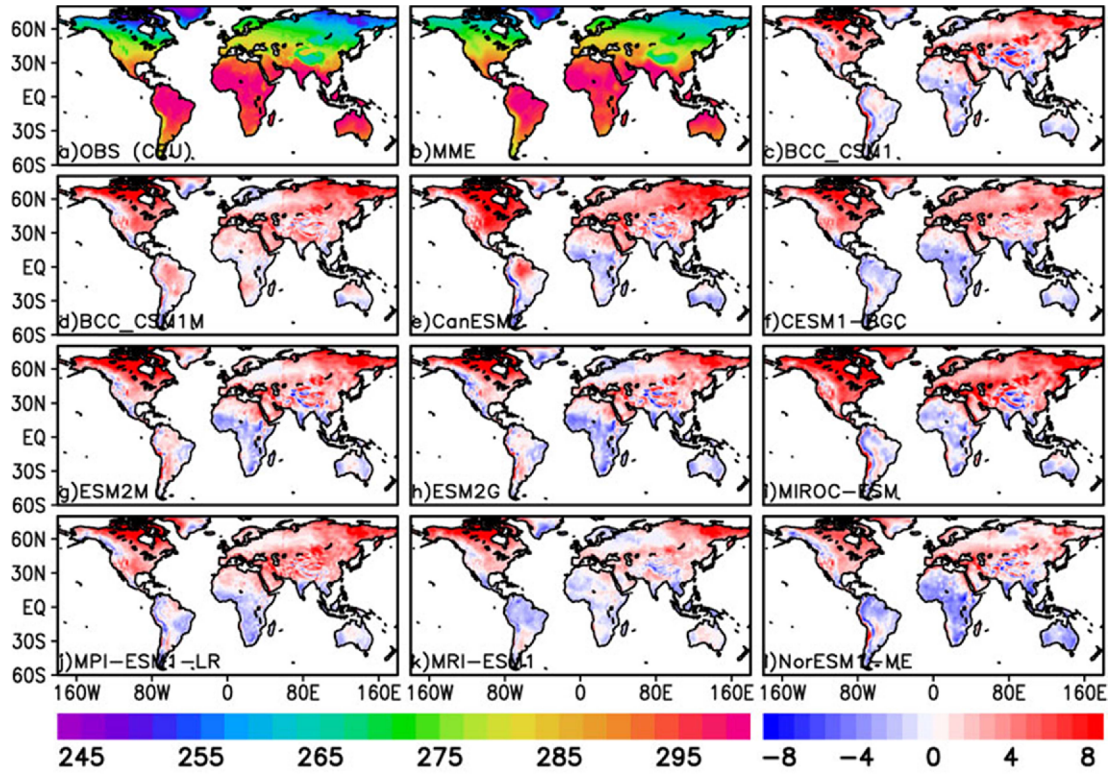


Fig. S1. Spatial distribution of annual-mean surface air temperature from the CRU observation (top left), MME (top middle) and the simulation bias in each model (model minus CRU). The unit is K.

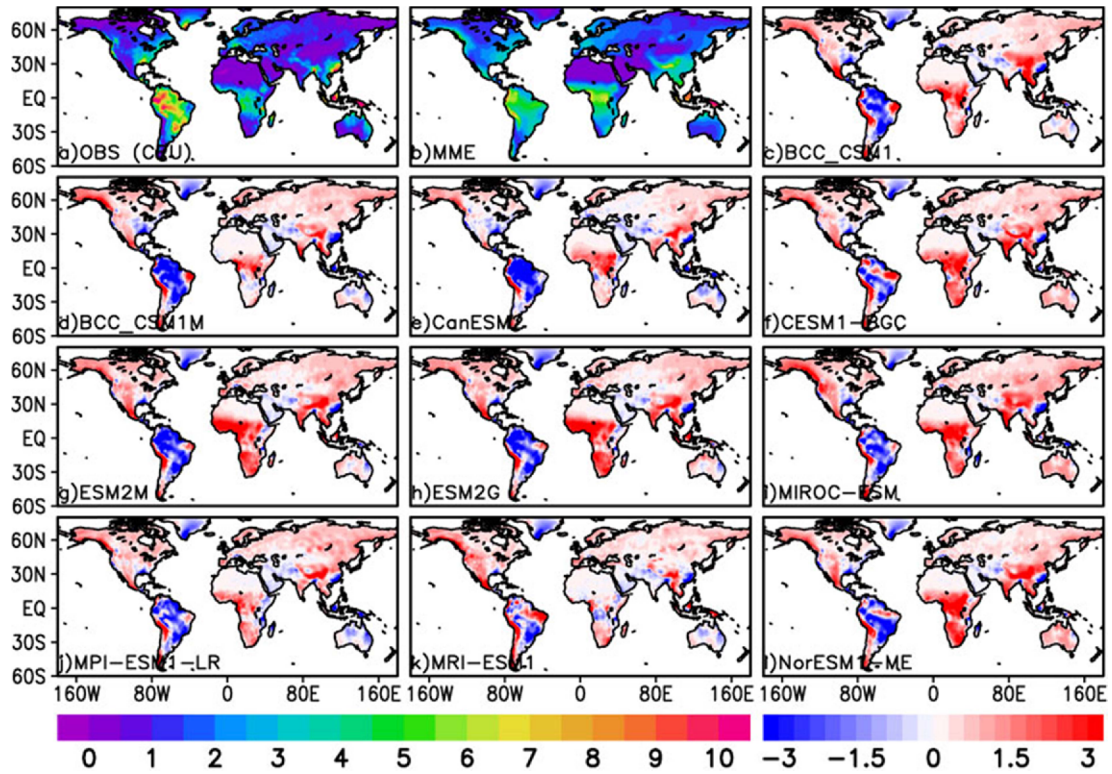
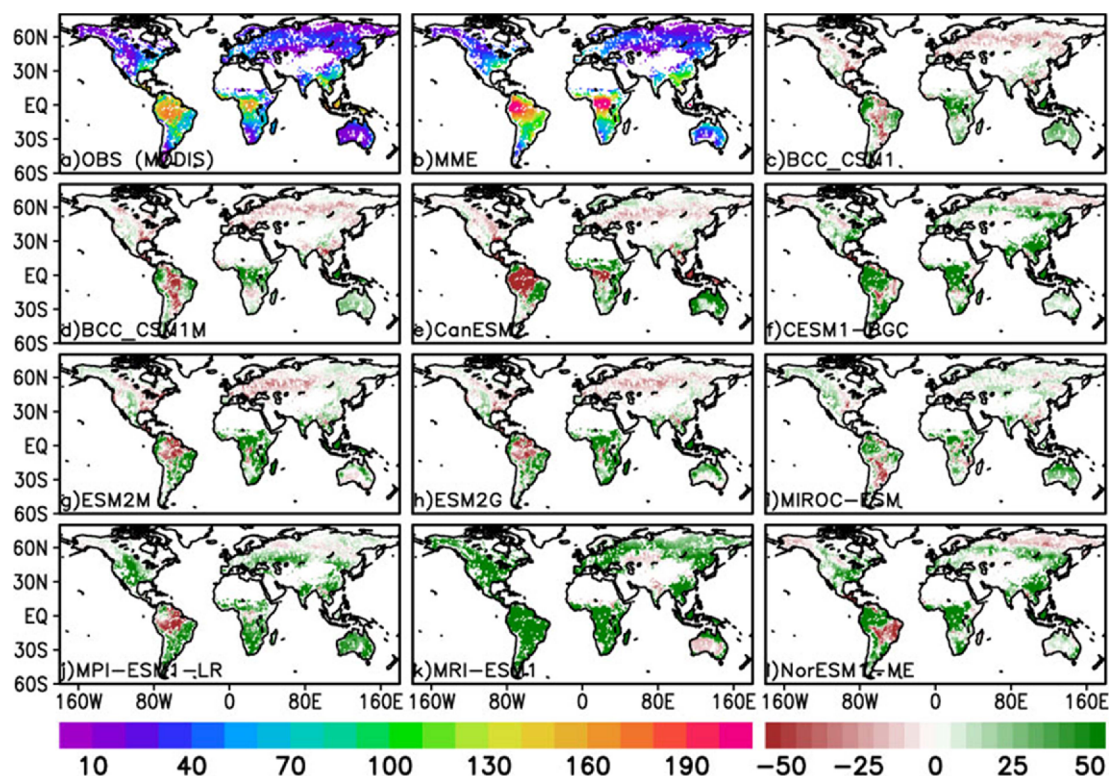


Fig. S2. Spatial distribution of annual-mean precipitation from the CRU observation (top left), MME (top middle) and the simulation bias in each model (model minus CRU). The unit is  $\text{mm d}^{-1}$ .





**Fig. S3.** Spatial distribution of annual  $R_a$  from the MODIS observation (top left), MME (top middle) and the simulation bias in each model (model minus MODIS). The unit is  $\text{gC m}^{-2} \text{mon}^{-1}$ .

## References

- Allen, C. D., and Coauthors, 2010: A global overview of drought and heat-induced tree mortality reveals emerging climate change risks for forests. *Forest Ecol. Manag.*, **259**, 660–684, doi:10.1016/j.foreco.2009.09.001.
- Amthor, J. S., 2000: The McCree-de Wit-Penning de Vries-Thornley respiration paradigms: 30 years later. *Ann. Bot.*, **86**, 1–20.
- Anav, A., and Coauthors, 2013: Evaluating the land and ocean components of the global carbon cycle in the CMIP5 Earth System Models. *J. Climate*, **26**, 6801–6843, doi:10.1175/JCLI-D-12-00417.1.
- Andres, R. J., J. S. Gregg, L. Losey, G. Marland, and T. A. Boden, 2011: Monthly, global emissions of carbon dioxide from fossil fuel consumption. *Tellus*, **63**, 309–327, doi:10.1111/j.1600-0889.2011.00530.x.
- Arnone III, J. A., and C. Körner, 1997: Temperature adaptation and acclimation potential of leaf dark respiration in two species of *Ranunculus* from warm and cold habitats. *Arctic Alp. Res.*, **29**, 122–125, doi:10.2307/1551842.
- Arora, V. K., and Coauthors, 2009: The effect of terrestrial photosynthesis down-regulation on the twentieth-century carbon budget simulated with the CCCma Earth System Model. *J. Climate*, **22**, 6066–6088.
- \_\_\_\_\_, and Coauthors, 2013: Carbon-concentration and carbon-climate feedbacks in CMIP5 earth system models. *J. Climate*, **26**, 5289–5314, doi:10.1175/JCLI-D-12-00494.1.
- Atkin, O. K., L. J. Atkinson, R. A. Fisher, C. D. Campbell, J. Zaragoza-Castells, J. W. Pitchford, F. I. Woodward, and V. Hurry, 2008: Using temperature-dependent changes in leaf scaling relationships to quantitatively account for thermal acclimation of respiration in a coupled global climate-vegetation model. *Glob. Change Biol.*, **14**, 2709–2726, doi:10.1111/j.1365-2486.2008.01664.x.
- Bond-Lamberty, B., and A. Thomson, 2010: Temperature-associated increases in the global soil respiration record. *Nature*, **464**, 579–582, doi:10.1038/nature08930.
- Booth, B. B. B., and Coauthors, 2012: High sensitivity of future global warming to land carbon cycle processes. *Environ. Res. Lett.*, **7**, 024002, doi:10.1088/1748-9326/7/2/024002.
- Choudhury, B. J., 2000: Carbon use efficiency, and net primary productivity of terrestrial vegetation. *Adv. Space Res.*, **26**, 1105–1108.
- Collatz, G. J., M. Ribas-Carbo, and J. A. Berry, 1992: Coupled photosynthesis-stomatal conductance model for leaves of  $C_4$  plants. *Funct. Plant Biol.*, **19**, 519–538, doi:10.1071/PP9920519.
- De Lucia, E. H., J. E. Drake, R. B. Thomas, and M. Gonzalez-Meler, 2007: Forest carbon use efficiency: Is respiration a constant fraction of gross primary production? *Glob. Change Biol.*, **13**, 1157–1167, doi:10.1111/j.1365-2486.2007.01365.x.
- Dewar, R. C., B. E. Medlyn, and R. E. McMurtrie, 1999: Acclimation of the respiration photosynthesis ratio to temperature: Insights from a model. *Glob. Change Biol.*, **5**, 615–622, doi:10.1046/j.1365-2486.1999.00253.x.
- Dunne, J. P., and Coauthors, 2012: GFDL's ESM2 global coupled climate-carbon Earth System Models Part II: Carbon system formulation and baseline simulation characteristics. *J. Climate*, **26**, 2247–2267, doi:10.1175/JCLI-D-12-00150.1.
- Enquist, B. J., A. J. Kerkhoff, S. C. Stark, N. G. Swenson, M. C. McCarthy, and C. A. Price, 2007: A general integrative model for scaling plant growth, carbon flux, and functional trait spectra. *Nature*, **449**, 218–222, doi:10.1038/nature06061.
- Farquhar, G. D., S. von Caemmerer, and J. A. Berry, 1980: A biochemical model of photosynthetic  $\text{CO}_2$  assimilation in leaves of  $C_3$  species. *Planta*, **149**, 78–90, doi:10.1007/BF00386231.
- Foley, J. A., I. C. Prentice, N. Ramankutty, S. Levis, D. Pollard, S. Stich, and A. Haxeltine, 1996: An integrated biosphere model of land surface processes, terrestrial carbon balance, and vegetation dynamics. *Global*

- Biogeochem. Cy.*, **10**, 603-628.
- Friedlingstein, P., I. Fung, E. Holland, J. John, G. Brasseur, D. Erickson, and D. Schimel, 1995: On the contribution of CO<sub>2</sub> fertilization to the missing biospheric sink. *Global Biogeochem. Cy.*, **9**, 541-556, doi:10.1029/95GB02381.
- \_\_\_\_\_, and Coauthors, 2006: Climate-carbon cycle feedback analysis: Results from the C4MIP model intercomparison. *J. Climate*, **19**, 3337-3353, doi:10.1175/JCLI3800.1.
- \_\_\_\_\_, M. Meinshausen, V. K. Arora, C. D. Jones, A. Anav, S. K. Liddicoat, and R. Knutti, 2014: Uncertainties in CMIP5 climate projections due to carbon cycle feedbacks. *J. Climate*, **27**, 511-526, doi:10.1175/JCLI-D-12-00579.1.
- Gifford, R. M., 1994: The global carbon-cycle - a viewpoint on the missing sink. *Funct. Plant Biol.*, **21**, 1-15, doi:10.1071/PP9940001.
- Giorgetta, M. A., and Coauthors, 2013: Climate and carbon cycle changes from 1850 to 2100 in MPI-ESM simulations for the Coupled Model Intercomparison Project phase 5. *J. Adv. Model. Earth Sy.*, **5**, 572-597, doi:10.1002/jame.20038.
- Harris, I., P. D. Jones, T. J. Osborn, and D. H. Lister, 2014: Updated high-resolution grids of monthly climatic observations - the CRU TS3.10 Dataset. *Int. J. Climatol.*, **34**, 623-642, doi:10.1002/joc.3711.
- Heinsch, F. A., and Coauthors, 2006: Evaluation of remote sensing based terrestrial productivity from MODIS using regional tower eddy flux network observations. *IEEE T. Geosci. Remote.*, **44**, 1908-1925, doi:10.1109/TGRS.2005.853936.
- Hoffman, F. M., and Coauthors, 2013: Causes and implications of persistent atmospheric carbon dioxide biases in Earth System Models. *J. Geophys. Res.*, **119**, 141-162, doi:10.1002/2013JG002381.
- Hurt, G. C., and Coauthors, 2011: Harmonization of land-use scenarios for the period 1500-2100: 600 years of global gridded annual land-use transitions, wood harvest, and resulting secondary lands. *Climatic Change*, **109**, 117-161, doi:10.1007/s10584-011-0153-2.
- Jung, M., and Coauthors, 2011: Global patterns of land-atmosphere fluxes of carbon dioxide, latent heat, and sensible heat derived from eddy covariance, satellite, and meteorological observations. *J. Geophys. Res.*, **116**, G00J07, doi:10.1029/2010JG001566.
- Knapp, A. K., J. T. Fahnestock, S. P. Hamburg, L. B. Statland, T. R. Seastedt, and D. S. Schimel, 1993: Landscape patterns in soil-plant water relations and primary production in tallgrass prairie. *Ecology*, **74**, 549-560.
- King, A. W., 2006: Atmosphere: Plant respiration in a warmer world. *Science*, **312**, 536, doi:10.1126/science.1114166.
- Larcher, W., and B. Mair, 1968: Das Kälteresistenzverhalten von *Quercus pubescens*, *Ostrya carpinifolia* und *Fraxinus ornus* auf drei thermisch unterschiedlichen Standorten. *Oecolog. Plantar.*, **3**, 255-270.
- Leith, C. E., 1975: Climate response and fluctuation dissipation. *J. Atmos. Sci.*, **32**, 2022-2026, doi:10.1175/1520-0469(1975)032<2022:CRAFD>2.0.CO;2.
- Long, M. C., K. Lindsay, S. Peacock, J. K. Moore, and S. C. Doney, 2013: Twentieth-century oceanic carbon uptake and storage in CEMS1 (BGC). *J. Climate*, **26**, 6775-6800, doi:10.1175/JCLI-D-12-00184.1.
- Mao, J., P. E. Thornton, X. Shi, M. Zhao, and W. M. Post, 2012: Remote sensing evaluation of CLM4 GPP for the period 2000-09. *J. Climate*, **25**, 5327-5342, doi:10.1175/JCLI-D-11-00401.1.
- Monteith, J., 1972: Solar radiation and productivity in tropical ecosystems. *J. Appl. Ecol.*, **9**, 747-766, doi:10.2307/2401901.
- Nemani, R. R., C. D. Keeling, H. Hashimoto, W. M. Jolly, S. C. Piper, C. J. Tucker, R. B. Myneni, and S. W. Running, 2003: Climate-driven increases in global terrestrial net primary production from 1982 to 1999. *Science*, **300**, 1560-1563, doi:10.1126/science.1082750.
- Obata, A., 2007: Climate-carbon cycle model response to freshwater discharge into the North Atlantic. *J. Climate*, **20**, 5962-5976, doi:10.1175/2007JCLI1808.1.
- Piao, S., P. Ciais, P. Friedlingstein, N. Noblet-Ducoudré, P. Cadule, N. Viovy, and T. Wang, 2009: Spatiotemporal patterns of terrestrial carbon cycle during the 20th century. *Global Biogeochem. Cy.*, **23**, GB4026, doi:10.1029/2008GB003339.
- \_\_\_\_\_, S. Luyssaert, P. Ciais, I. A. Janssens, A. Chen, C. Cao, J. Fang, P. Friedlingstein, Y. Luo, and S. Wang, 2010: Forest annual carbon cost: A global-scale analysis of autotrophic respiration. *Ecology*, **91**, 652-661, doi:10.1890/08-2176.1.
- Rahman, A. F., D. A. Sims, V. D. Cordova, and B. Z. El-Masri, 2005: Potential of MODIS EVI and surface temperature for directly estimating per-pixel ecosystem C fluxes. *Geophys. Res. Lett.*, **32**, L19404, doi:10.1029/2005GL024127.
- Running, S. W., and S. T. Gower, 1991: FOREST-BGC, a general model of forest ecosystem processes for regional applications. II. Dynamic carbon allocation and nitrogen budgets. *Tree Physiol.*, **9**, 147-160, doi:10.1093/treephys/9.1-2.147.
- Ryan, M. G., 1991: Effects of climate change on plant respiration. *Ecol. Appl.*, **1**, 157-167, doi:10.2307/1941808.
- Shao, P., X. Zeng, K. Sakaguchi, R. K. Monson, and X. Zeng, 2013: Terrestrial carbon cycle: climate relations in eight CMIP5 earth system models. *J. Climate*, **26**, 8744-8764, doi:10.1175/JCLI-D-12-00831.1.
- Taylor, K. E., 2001: Summarizing multiple aspects of model performance in a single diagram. *J. Geophys. Res.*, **106**, 7183-7192, doi:10.1029/2000JD900719.
- \_\_\_\_\_, R. J. Stouffer, and G. A. Meehl, 2012: An overview of CMIP5 and the experiment design. *Bull. Amer. Meteor. Soc.*, **93**, 485-498, doi:10.1175/BAMS-D-11-00094.1.
- Tjiputra, J. F., C. Roelandt, M. Bentsen, D. M. Lawrence, T. Lorentzen, J. Schwinger, Ø. Seland, and C. Heinze, 2013: Evaluation of the carbon cycle components in the Norwegian Earth System Model (NorESM). *Geosci. Model Dev.*, **6**, 301-325, doi:10.5194/gmd-6-301-2013.
- Tucker, C. L., J. Bell, E. Pendall, and K. Ogle, 2013: Does declining carbon-use efficiency explain thermal acclimation of soil respiration with warming? *Glob. Change Biol.*, **19**, 252-263, doi:10.1111/gcb.12036.
- Turner, P. D., W. D. Ritts, M. Zhao, S. A. Kurc, A. L. Dunn, S. C. Wofsy, E. E. Small, and S. W. Running, 2006: Assessing interannual variation in MODIS-based estimates of gross primary production. *IEEE T. Geosci. Remote.*, **44**, 1899-1907.
- Todd-Brown, K. E. O., J. T. Randerson, W. M. Post, F. M. Hoffman, C. Tarnocai, E. A. G. Schuur, and S. D. Allison, 2013: Causes of variation in soil carbon simulations from CMIP5 earth system models and comparison with observations. *Biogeosci.*, **10**, 1717-1736, doi:10.5194/bg-10-1717-2013.
- Watanabe, S., and Coauthors, 2011: MIROC-ESM 2010: Model description and basic results of CMIP5-20c3m experiments. *Geosci. Model Dev.*, **4**, 845-872, doi:10.5194/gmd-4-845-2011.
- Williams, D. N., B. N. Lawrence, M. Lautenschlager, D. Middleton, and V. Balaji, 2011: The earth system grid federation: Delivering globally accessible petascale data for CMIP5. *Proc. Asia-Pac. Adv. Network*, **32**, 121-130, doi:10.7125/APAN.32.15.
- Woodwell, G. M., 1990: The effects of global warming. In *Global Warming: The Greenpeace Report*, J. Leggett Ed., Oxford University Press, 116-132.
- Wu, T., and Coauthors, 2013: Global carbon budgets simulated by the Beijing Climate Center Climate System Model for the last century. *J. Geophys. Res.*, **118**, 4326-4347, doi:10.1002/jgrd.50320.
- Yang, W., N. V. Shabanov, D. Huang, W. Wang, R. E. Dickinson, R. R. Nemani, Y. Knyazikhin, and R. B. Myneni, 2006: Myneni Analysis of leaf area index products from combination of MODIS Terra and Aqua data. *Remote Sens. Environ.*, **104**, 297-312, doi:10.1016/j.rse.2006.04.016.
- Yukimoto, S., and Coauthors, 2011: Meteorological Research Institute-Earth System Model Version 1 (MRI-ESM1): Model description.

- Technical Reports of the Meteorological Research Institute No.64, 88 pp, doi:10.11483/mritechrepo.64.
- Zaehle, S., and Coauthors, 2014: Evaluation of 11 terrestrial carbon-nitrogen cycle models against observations from two temperate Free-Air CO<sub>2</sub> Enrichment studies. *New phytol.*, **202**, 803-822, doi:10.1111/nph.12697.
- Zha, T. S., and Coauthors, 2013: Gross and aboveground net primary production at Canadian forest carbon flux sites. *Agricul. Forest Meteorol.*, **174**, 54-64, doi:10.1016/j.agrformet.2013.02.004.
- Zhang, Y., M. Xu, H. Chen, and J. Adams, 2009: Global pattern of NPP to GPP ratio derived from MODIS data: Effects of ecosystem type, geographical location and climate. *Glob. Ecol. Biogeogr.*, **18**, 280-290, doi:10.1111/j.1466-8238.2008.00442.x.
- \_\_\_\_\_, G. Yu, J. Yang, M. C. Wimberly, X. Zhang, J. Tao, Y. Jiang, and J. Zhu, 2014: Climate-driven global changes in carbon use efficiency. *Glob. Ecol. Biogeogr.*, **23**, 144-155, doi:10.1111/geb.12086.
- Zhao, F., and N. Zeng, 2014: Continued increase in atmospheric CO<sub>2</sub> seasonal amplitude in the 21st century projected by the CMIP5 Earth System Models. *Earth Syst. Dynam.*, **5**, 423-439, doi:10.5194/esd-5-423-2014.
- Zhao, M. S., F. A. Heinsch, R. R. Nemani, and S. W. Running, 2005: Improvements of the MODIS terrestrial gross and net primary production global data set. *Remote Sens. Environ.*, **95**, 164-176, doi:10.1016/j.rse.2004.12.011.
- Zhu, Q., and Q. Zhuang, 2015: Ecosystem biogeochemistry model parameterization: Do more flux data result in a better model in predicting carbon flux? *Ecosphere*, **6**, 1-20, doi:10.1890/ES15-00259.1.